SCIENCE CHINA
Technological Sciences

October 2010 Vol.53 No.10: 2867–2877
doi: 10.1007/s11431-010-4046-9

Analytical method for softness abrasive flow field based on discrete phase model

JI ShiMing[1,2], XIAO FengQing[1,2] & TAN DaPeng[1,2*]

[1]*Key Laboratory of Special Purpose Equipment and Advanced Manufacturing Technology, (Zhejiang University of Technology), Ministry of Education, Hangzhou 310014, China;*
[2]*Key Laboratory of Special Purpose Equipment and Advanced Manufacturing Technology of Zhejiang Province, Hangzhou 310014, China;*

Received April 1, 2010; accepted June 17, 2010

Aiming at the problem of difficult contact finishing for mini structural surface in course of mould manufacturing, a new no-tool precision machining method based on soft abrasive flow machining (SAFM) was proposed. It allocated restrained component near surface machined, constituted restrained abrasive flow passage, and made the surface become a segment of passage wall. It could control turbulence abrasive flow in restrained passage, realize micro cutting for passage wall, and utilize the irregular motion of abrasive flow to eliminate the mono-directional marks on machined surfaces, and the precision could reach the specular level. A two-phase dynamic model of abrasive flow oriented to SAFM combined with discrete phase model (DPM) was established, the law of two-phase flow motion and the related physical parameters was obtained by corresponding numerical simulation method, and the mechanism of precision machining in SAFM was discussed. Simulation results show that the abrasive flow machining process mainly appears as translation of ablating location with the influence by granular pressure, and as the variation of machining efficiency with the influence by near-wall particle velocity. Thus via control of the inlet velocity and its corresponding machining time, it is supposed to work out the machining process according to the machining requirements by using the Preston equation to seek the relationship among velocity, pressure and material removing rate. By tracking near-wall particles, it can be confirmed that the movement of near-wall abrasive particles is similar to stream-wise vortices. The cutting traces on workpiece surfaces assume disorderly arrangement, so the feasibility of the SAFM method can be reaffirmed.

structural flow passage, ultra-precision machining, softness abrasive flow, discrete phase model

Citation: Ji S M, Xiao F Q, Tan D P. Analytical method for softness abrasive flow field based on discrete phase model. Sci China Tech Sci, 2010, 53: 2867–2877, doi: 10.1007/s11431-010-4046-9

1 Introduction

With leaps and bounds of computer performance, and the generation of massively parallel computation, feasibility and necessity of simulated calculation for engineering questions have drawn more attention. As a classical subject, fluid mechanics has been infused with new life and energy from these benefits, and its application has been penetrating into every fields of basic industry [1].

Presently, research on functional fluid limits only in situations like circular or rectangle tube channels, which makes it convenient to work out several basic flow characteristics. Yet in practical applications, besides these conventional channels, there are lots of abnormally shaped channels. The functional fluid flow situation in these abnormal channels has rarely been studied in recent researches [2]. As for the precision machining of grooves, holes, prisms, pyramids, narrow channels involved in mould manufacturing, conventional abrasive manu-

*Corresponding author (email: tandapeng@zjut.edu.cn)

facture methods have an extremely limited range of application, and are mainly manifested in the inability of machining small-dimension complex structural surfaces with hard physical cutting tools. To solve this problem, Extrude Hone Corporation of USA invented and patented the abrasive flow machining (AFM) process in 1966, which was firstly applied to the deburring processing of alloyed workpieces with complex geometry in aerospace field. In an AFM process, abrasive particles in fluid media are used as cutting tools acting on machining surfaces repeatedly in a finishing processing. And its precision can reach up to 0.05 μm. AFM ensures high-quality machined surfaces as well as a closure tolerance under an economical processing speed [3]. Abrasive flow is a precision machining method adapting to different machining shapes. It is mainly applied to precision machining involving the processing of interior complex structure of workpieces, especially in sophisticated high-technology field, such as the manufacture of turbine blades and straightener blades in aerospace field, injection ion nozzles, pumps and expansion valve bodies in automotive field, membranes valves and pumps in medical appliance field, grooved drum guide wire in textile field and moulds and products in other fields [4]. Through decades of development, the mechanism, processing technique and application of AFM have attracted wide attention of many researchers.

Conventional AFM methods are mainly refer to abrasive jet machining (AJM) and extrusion hone. AJM is mainly applied in lapping of brittle and hard materials. A widely applied method of AFM at present is to force an abrasive viscoelastic laden media across workpiece surface under certain pressure in finishing procedure [5]. These methods mentioned above are comparatively mature in techniques. However, since the removal amount is difficult to control and the cutting is equi-directional, the machining precision can hardly be improved. Yet there are several modified AFM methods giving improvement to AFM in machining precision and controllability. Micro Technica Technologies developed an AFM method using a semi-liquid paste. Madadnia and Reizes suggested to carry abrasive particles in bubbles in fluid media, and take advantage of near-wall cavitations to produce impact erosions on workpiece surfaces [6]. Besides, there are several methods which combine AFM with other processing methods, such as ultrasonic flow polishing [7], vibration polishing [8], magnetorheological abrasive flow finishing [9] and so on.

Soft Abrasive Flow Machining (SAFM) is one of these methods. In SAFM, turbulence is generated in abrasive fluid across workpiece surfaces. It is supposed to achieve poly-directional and multi-angle cuttings on surface of the workpiece by utilizing the irregular motion of ablating particles. Thus as the mono-directional marks on the machined surfaces were eliminated by homogeneous abrasion, the precision could finally reach the specular level.

The mechanism of AFM is not complicated, but it has numerous influence factors and machining parameters，such as cycle loops, abrasive concentration, fluid velocity, passage pressure, boundary conditions, and so on [3]. Therefore, it is necessary to develop an appropriate two-phase flow research method to analyze and predict the situation of surface machining in fluid bed, and lay the foundations for the design of working passage and guidance block. As for the solid-fluid flow, except for the coupling of motion of particle phase and fluid phase, the collision between particles should be considered as well. For this reason, the motion of particles in two-phase flow is a comparatively complex process. However, as for the dilute two-phase flow with a volume fraction that is small enough, the space between abrasive particles is big enough to have the collision ignored, which means the motion of particles can be simplified. Discrete phase model (DPM) is a two-phase flow research method oriented to dilute flow. In this paper, the mechanism of mould structural surface polishing method based on DPM was investigated, and the situation in the passage was simulated using software Fluent.

2 DPM oriented to SAFM

In a solid-fluid flow, DPM is introduced to simplify the simulation of motion of particle phase. When volume fraction of the particle phase is small enough, interaction between particles can be considered absent, which means the volume fraction of discrete phase must be considerably small, regularly less than 10%−12% [10, 11]. Under these circumstances, a DPM can be used to calculate trajectories of a portion of particles in discrete phase, and nevertheless a simulation of particle motion with universal application value can be obtained. It is possible to simulate motion tracks and collision characteristics at single-particle level, and lead to great simplification in the calculation process.

2.1 Mathematical model description

Since the mixed fluid studied in this paper is incompressible, multiphase Eulerian model formulations are acceptable in this case. The continuity equation and momentum equation of phase q are respectively expressed as below:

$$\frac{\partial}{\partial t}(\alpha_q \rho_q) + \nabla \cdot (\alpha_q \rho_q \boldsymbol{v}_q) = \sum_{p=1}^{n} \dot{m}_{pq} , \tag{1}$$

$$\frac{\partial}{\partial t}(\alpha_q \rho_q \boldsymbol{v}_q) + \nabla \cdot (\alpha_q \rho_q \boldsymbol{v}_q \boldsymbol{v}_q) = -\alpha_q \nabla p + \nabla \cdot \overline{\overline{\tau}}_q + \sum_{p=1}^{n} (\boldsymbol{R}_{pq} + \dot{m}_{pq} \boldsymbol{v}_{pq}) + \alpha_q \rho_q \boldsymbol{F}_q , \tag{2}$$

where ρ_q is density of fluid phase, $\boldsymbol{v}_q$ is velocity of fluid phase, $\dot{m}_{pq}$ is mass transfer from solid phase to fluid phase, p is pressure of mixed fluid, $\boldsymbol{R}_{pq}$ is interaction between phases, $\boldsymbol{F}_q$ is external body force. $\overline{\overline{\tau}}_q$ is pressure strain

tensor stated as

$$\overline{\overline{\tau}}_q = \alpha_q \mu_q \left(\nabla \boldsymbol{v}_q + \nabla \boldsymbol{v}_q^T\right) + \alpha_q \left(\lambda_q - \frac{2}{3}\mu_q\right)\nabla \cdot \boldsymbol{v}_q \overline{\overline{I}}, \quad (3)$$

where μ_q is shear viscosity, λ_q is volume viscosity. In eqs. (2) and (3), α_q is volume fraction of particle phase stated as

$$\alpha_q = 1 - \sum_{i=1}^{n} V_{pi} / \Delta V, \quad (4)$$

where V_{pi} and ΔV are respectively volume of control volume and volume of particle *i*. In most cases, turbulence model involves a group of partial differential equations unrelated to time. Therefore, it is easy to derive discrete model of particle phase from Eulerian model. In two-phase flow the particle phase is calculated as a continuous phase mixed in the fluid. Motion of particle phase can also be solved via a group of conservation equations of continuous phase. Transport equations of particle phase, such as continuous equations and momentum equations, can all be derived from the differential equations of fluid phase [12].

The solution procedure of Eulerian particle model is in practice a procedure of iterative. A grief advantage of Eulerian particle model lies in its convenience of executing, solving and explanation in fluid phase equations [13]. The numerical computation method of fluid phase equations can also be utilized in the solution of particle phase.

Trajectories of particles can be obtained by integration for force equilibrium equation of particle at Lagrangian coordinates. The force equilibrium of particle indicates a equilibrium between particle inertia force and external force. Motion equation for spherical particle is stated as

$$\begin{aligned}\text{Inertia force} = {} & \text{Steady drag force} + \text{Basset} \\ & + \text{Virtual mass force} + \text{Magnus} \\ & + \text{Body force/Gravity} - \text{buoyancy}\end{aligned} \quad (5)$$

In mechanical engineering field, steady drag force in eq. (5) is the key component in the force loading on particle. In majority of dilute particle flow, turbulence intensity is less than 20% with density ratio of solid-fluid flow larger than 200, and the characteristic scale is smaller than Kolmogorov scale. Therefore, the particles can be treated as spheres. Under these conditions, motion equation of particle phase can be greatly simplified, by ignoring all the forces but gravity and drag force [14]. The simplified motion equation without Basset, Virtual mass force, Magnus, Saffman and buoyancy is stated as below (*x* direction at Cartesian coordinate):

$$\frac{\mathrm{d}u_p}{\mathrm{d}t} = \frac{1}{\tau_p}\left(u - u_p\right) + \frac{g_x(\rho_p - \rho)}{\rho_p}, \quad (6)$$

where u is the velocity of fluid phase, u_p is the particle velocity, g_x complementary acceleration (force acting on particles per unit mass), and τ_p particle relaxation time, which is stated as below, according to the equation introduced by Manninen et al.:

$$\tau_p = \frac{\rho_p d_p^2}{18\mu} \frac{24}{C_{\mathrm{D}} Re}, \quad (7)$$

where μ is the molecular viscosity of fluid, ρ_p is granular density, d_p is granular diameter, and *Re* is relative Reynolds number, which is stated as

$$Re = \frac{\rho d_p \left|\boldsymbol{u}_p - \boldsymbol{u}\right|}{\mu}. \quad (8)$$

And C_{D} is drag coefficient defined by the model, stated as

$$C_{\mathrm{D}} = \left(0.63 + \frac{4.8}{\sqrt{Re_s / v_{r,s}}}\right)^2. \quad (9)$$

This model is derived from terminal velocity of the particle in fluidized bed. Terminal velocity is related to volume fraction and Reynolds number. Solid-fluid exchange coefficient is stated as

$$K_{\mathrm{sl}} = \frac{3\alpha_s \alpha_l \rho_l}{4 v_{r,s}^2 d_s} C_{\mathrm{D}} \left(\frac{Re_{\mathrm{s}}}{v_{r,s}}\right)\left|\boldsymbol{v}_s - \boldsymbol{v}_l\right|. \quad (10)$$

In eqs. (9) and (10), $v_{r,s}$ is terminal velocity related to velocity of solid phase.

$$\begin{aligned} v_{r,s} = {} & 0.5(A - 0.06Re \\ & + \sqrt{\left(0.06Re_{\mathrm{s}}\right)^2 + 0.12Re_s\left(2B - A\right) + A^2}), \end{aligned} \quad (11)$$

where $A = \alpha_l^{4.14}$, $B = \begin{cases} 0.8\alpha_l^{1.28}, & \alpha_l \leqslant 0.85, \\ \alpha_l^{2.65}, & \alpha_l > 0.85. \end{cases}$

Particle distribution was simulated with stochastic trajectory model, in which each injection is tracked repeatedly in order to generate a statistically meaningful sampling. And mass flow rates and exchange source terms for each injection are divided equally among multiple stochastic tracks.

Turbulent fluctuations in the flow field are represented by defining an instantaneous fluid velocity:

$$u_i = \overline{u}_i + u'_i, \quad (12)$$

where $\overline{u}_i$ is the mean velocity of fluid phase, while u'_i is derived from local turbulence parameters:

$$u'_i = \zeta \sqrt{\frac{2k}{3}}, \quad (13)$$

where k is turbulent kinetic energy, and ζ is a normally dis-

tributed random number.

Wall condition of the particle is given in Figure 1. For particle reflection, a restitution coefficient e is specified:

$$\begin{cases} e_n = \dfrac{v_{2,n}}{v_{1,n}}, \\ e_t = \dfrac{v_{2,t}}{v_{1,t}}, \end{cases} \tag{14}$$

where $v_{1,n}$ is the normal component of velocity before the collision, $v_{2,n}$ is the normal component of velocity after the collision, $v_{1,t}$ is the tangential component of velocity before the collision, $v_{2,t}$ is the tangential component of velocity after the collision. Coefficient of restitution is the ratio of differences in velocities before and after the collision. A restitution coefficient is regular in between [0,1]. For elastic collision, restitution coefficient is 1, while restitution coefficient of perfect inelastic collision is 0.

Considering that the motion of abrasive particles located in laminar sublayer is the primary motion in the SAFM method, near-wall mesh is enriched enough to be able to resolve with enhanced wall treatment method. Using a function suggested by Kader [15], situation of laminar sublayer of turbulence flow can be simulated. Thereby movement and trajectories of working abrasive particles can then be evaluated. For details see Section 2.3.

2.2 Mathematical model description

In this paper, the straight passage, with a length of 50 mm, is formatted by machining surfaces and the restrained module. The restrained module can limit dimensions of the passage, and consequently affect environment parameters of flow field (pressure, flow rate, turbulence intensity etc.). Both the restrained module and the workpiece are strictly located and clamped. The cross section is described in Figures 2–4 (unit: mm):

The model is meshed in hexagonal unstructured grids with total grid number approx 80000 (shown in Figure 5). Choose velocity inlet and overflow outlet as the boundary conditions. The fluid phase is engine oil, with a density of 880 kg/m^3 and a viscosity of 46×10^{-6} m^2/s. The particle phase uses SiC as its material, and its density and kinetic viscosity are respectively 3170 kg/m^3 and 2.064×10^{-6} m^2/s. Average granular diameter is 55 μm. Volume fraction of the particle phase is 0.1. A group of particle injection directing perpendicularly to the inlet face is set to inlet of the passage. Solve the problem with second-order upwind pressure-velocity coupled Phase Coupled SIMPLE algo-

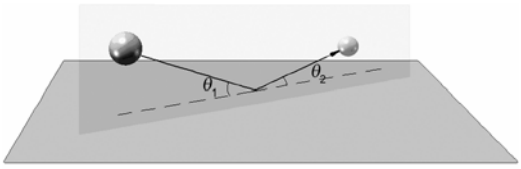

Figure 1 Particle reflection.

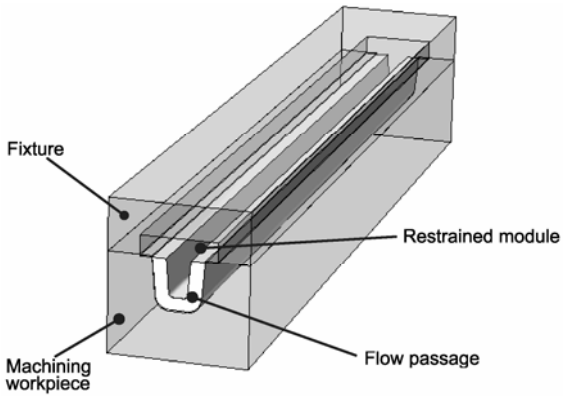

Figure 2 Geometry structure of structural flow passage.

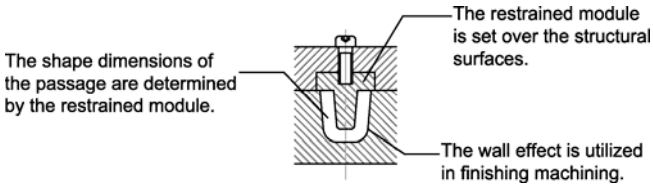

Figure 3 Mechanism of SAFM.

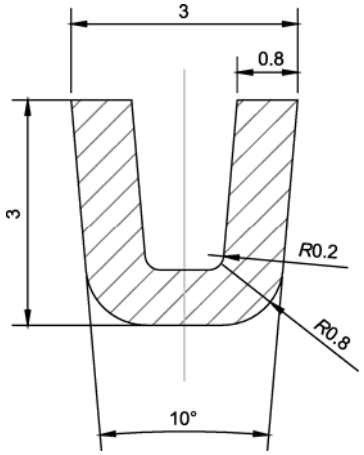

Figure 4 Cross section of structural flow passage.

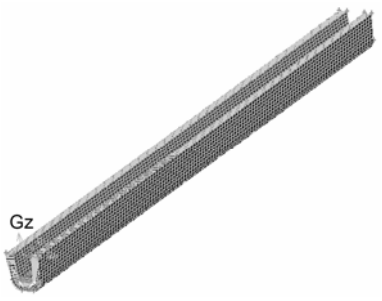

Figure 5 Mesh generation of the passage.

rithm. Iteration step is set to 0.0001 s.

3 Computational results and analysis

3.1 Setting of initial parameters

Material removal types can be divided into 2 categories: brittle removal and ductile removal. Polishing with abrasive flow is a very complicated removal process, which involves collision and cuttings of the particle acting on workpiece materials [16, 17]. In the SAFM cases, constant proportion coefficient among load, velocity and removal varies along with change of the workpiece or abrasive situation or machining methods/shapes [18]. A basic physical expression of material removal, namely Preston equation, was given to show that removal rate is not only proportional to pressure and linear velocity, but also suggests some other physical and chemical properties and some machinery parameters and characters, which can be expressed as

$$R = K_{\mathrm{p}} P V , \tag{15}$$

where R is removal rate, P is pressure acting on workpiece, V is the relative linear velocity, and K_{p} is Preston constant [19]. Since Preston equation expresses proportionality of the removal rate to pressure and linear velocity, in SAFM, pressure P exerted on workpiece surfaces is practically the granular pressure acting on workpiece surfaces, and V can be substituted by longitudinal velocity of particles in near-wall regions. Thus granular pressure and particle velocity were collected to find the expression of removal rate variety of longitudinal softness abrasive flow.

Granular pressure is the additional pressure exerted on the walls of a fluidized bed due to particle collisions with that wall [20]. It is the direct reason of ablating on passage surfaces, and can be stated as

$$P_p = \frac{2}{3}\alpha_p \rho_p q_p^2 \left[1 + 2\alpha_p g_0 \left(1 + e_{\mathrm{c}}\right)\right], \tag{16}$$

where q_p^2 is the fluctuating kinetic energy of particles, e_{c} is normal coefficient of restitution of Collisions, and g_0 is pair correlation function stated as

$$g_0 = \left(1 - \alpha_p / \alpha_{p,m}\right)^{-2.5\alpha_{p,m}} . \tag{17}$$

From eq. (16), granular pressure is linked to fluctuating kinetic energy of near-wall particle phase and its distribution. In the SAFM cases, granular pressure comprehensively indicates abrasive efficiency and intensity. Since the ultimate purpose of AFM is to achieve more evenly machined surfaces, granular pressure distribution curve is chosen to be the primary research object. It is believed that granular pressure exerted on machining surfaces must be relevant to ultimate abrasive removal.

In 1933 Nikuradse found from the formulas for near-wall laminar sublayer height that linear loss coefficient was a function of Reynolds number *Re* and relative roughness factor [21]. Experiments with circular tubes with different roughness factors show that to form a steady near-wall turbulence, a much higher Reynolds number is desirable on a smooth surface, compared with that on a rough one. Considering that roughness of machining surface is rather low (Ra=0.01 μm), it is proper to use a higher Reynolds number to produce a more stable near-wall turbulence flow. And because Reynolds number is influenced by inlet velocity, initial conditions listed in Table 1 are used for simulation. When inlet velocity is higher than or equal to 90 m/s, turbulence is considered to be generated in the passage.

3.2 Simulation results and analysis

From the passage wall (Note: In this paper the wall refers in particular to machining surfaces. The same below.) chose 10 sampling points along the passage on *XY* plane for analysis (see Figure 6). Figure 7 shows volume fraction distribution of near-wall particle phase under different Reynolds numbers. Results can be seen that after particle flow enters the passage, the particles tend to travel away from wall, converging on interlayer between the walls. After they have covered a distance of d, flow condition in the passage goes stabilized, and particle phase becomes better distributed, which makes its near-wall volume fraction tend to be more constant. In laminar conditions, value of d equals approximately to 10 mm. While Reynolds number is set within turbulence scale, and inlet velocity should thereby be

Table 1 Initial parameters in simulation

Inlet velocity (m/s)	Reynolds number
60	2080
70	2427
80	2773
90	3120
100	3467
110	3814
120	4160
130	4507
140	4857
150	5201

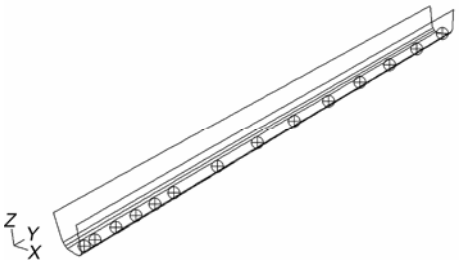

Figure 6 Sampling points on bottom wall.

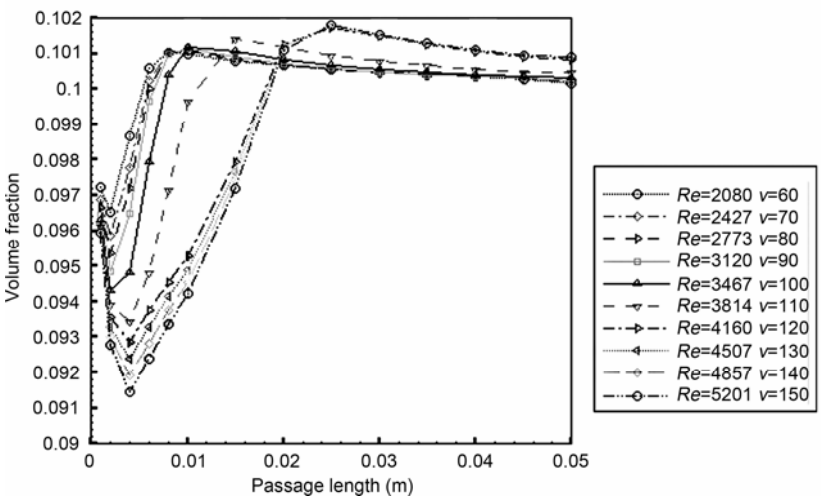

Figure 7 Particle volume fraction distribution under different Reynolds numbers.

higher, thus it will take a longer d for particles to be well-distributed. When Reynolds number goes up to 4000 and above, d will reach a constant value of 20 mm. As for machining surfaces, since cutting capacity of particles is considered to be equal, a higher volume fraction signifies a larger number of particles working. That is a higher abrasive efficiency namely. And obviously, areas with the same particle volume fraction would gain corresponding abrasive results. Figure 8 shows particle volume fraction contour given the initial inlet velocity of 130 m/s and a Reynolds number of 4507.

Figure 9 gives turbulence fluctuating kinetic energy distribution curve under different Reynolds numbers. Turbulence fluctuating kinetic energy indicates fluctuating length and its time scale. Apparently turbulence fluctuating kinetic energy improves along with its Reynolds number, and so does the abrasive intensity. Kinetic energy would not change much in the passage after a distance of 5 mm, which means cutting capacity of particle can be treated as constant.

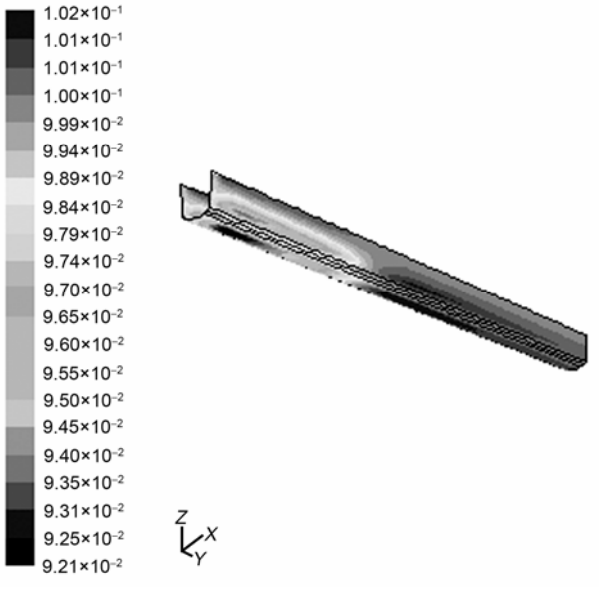

Figure 8 Particle volume fraction contour with Re=4507.

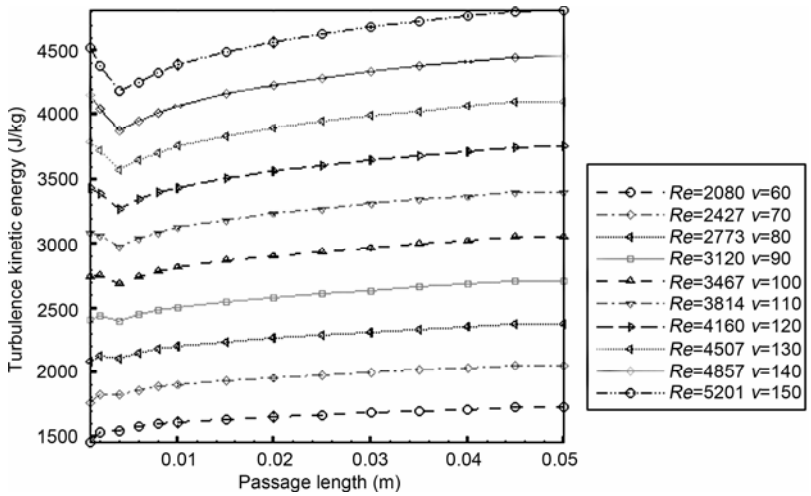

Figure 9 Turbulence fluctuating kinetic energy distribution under different Reynolds numbers.

Figure 10 shows kinetic energy contour given the initial inlet velocity of 130 m/s and a Reynolds number of 4507.

Figure 11 gives near-wall granular pressure distribution curve. It can be noticed that after a turbulence formed in two-phase flow, granular pressure enters an interval where its value is apparently constant. According to the theories mentioned above, in this interval abrasive results can be regarded as equal. Moreover, along with the increase of Reynolds number and particle volume fraction, granular pressure presents increased development trends as turbulence fluctuating kinetic energy [22]. After that, due to the increase of fluctuating intensity, dynamic pressure of particle phase grows with it. Thereby granular conductivity (equal to diffusion coefficient k_{Θ_s} of particle phase in FLUENT) tends to go down. For flow fields whose Reynolds numbers lower than 4000, granular pressure will soon get restrained by decreasing diffusivity, and consequently result in decreasing of granular pressure. Yet if Reynolds number is higher, turbulence kinetic energy will own more control of granular pressure, making a larger interval in which the granular pressure value can keep constant till end of the passage. Therefore, for passages with a higher Reynolds number, the first 20 mm is considered as preparing area, and the next 30 mm is working area, and more evenly and stably machining results can be seen in the latter.

Similarly, choose another two sets of sampling points on the side and corner respectively (as shown in Figure 12). The related data is analyzed and results are just about the same. Figures 13 and 14 show respectively volume fraction and granular pressure distribution curves of samples initialized with an inlet velocity of 130 m/s and a Reynolds number of 4507. Influenced by shape of passage and deposition, granular pressure exerted on side walls can be much more stable than it on bottom wall. The conditions of side walls are favorable to formation of turbulence, making it possible for granular pressure to reach a stable level in a shorter distance. Hence, it is believed that machining results will be better on side walls, which means, machining efficiency on bottom wall is still the prime case in the SAFM method.

Another important variable in Preston equation is removal rate. Since in FLUENT particle velocity on solid boundaries is set to zero, in this paper the most-near-wall particles were chosen to provide their longitudinal velocity as a substitute of collision velocity onto the wall. Figure 15 shows velocity distribution under different Reynolds numbers. Influenced by passage shape, particle injection meets a big jam at around the inlet surface, and this situation would become severer when inlet velocity grows. After this procedure, particle flow turns stable, and under the influence of resistances like friction, longitudinal velocity of particles starts to decrease gradually till the end of the passage. It can be concluded from Figure 15 that the curve line features with different velocities are basically the same, with their curvatures staying generally invariable. Therefore, it is easy to infer that near-wall particle flow rate (namely particle

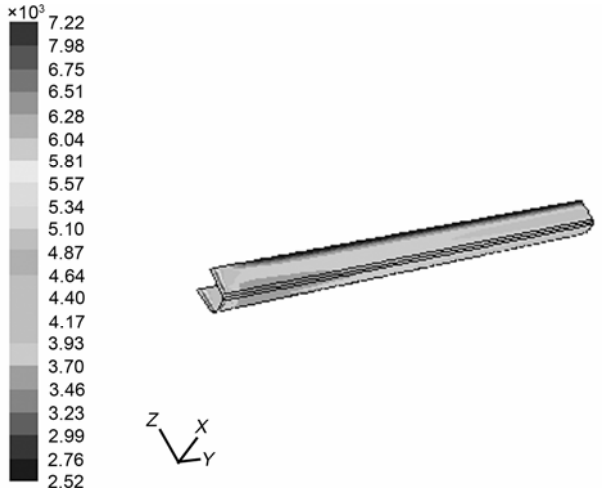

Figure 10 Kinetic energy contour with *Re*=4507.

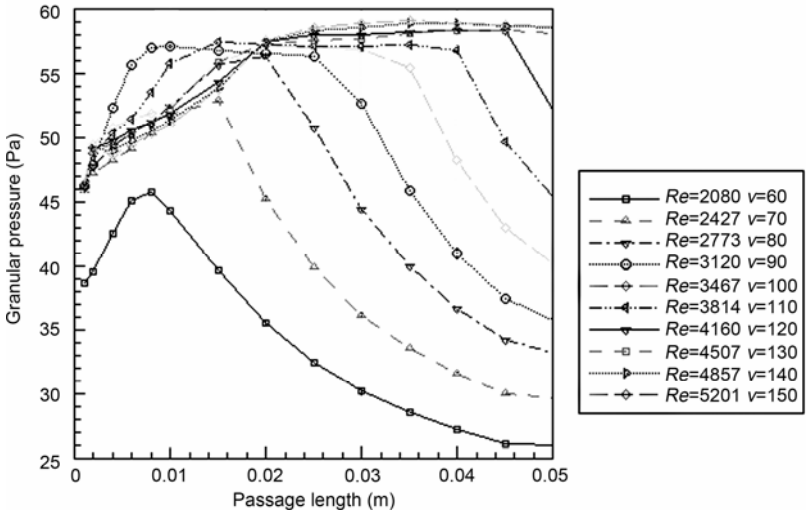

Figure 11 Granular pressure distribution under different Reynolds numbers.

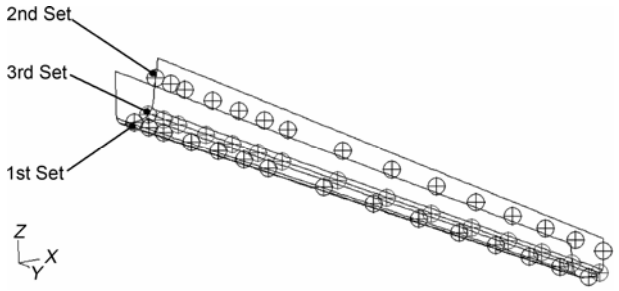

Figure 12 Sets of sampling points in the passage.

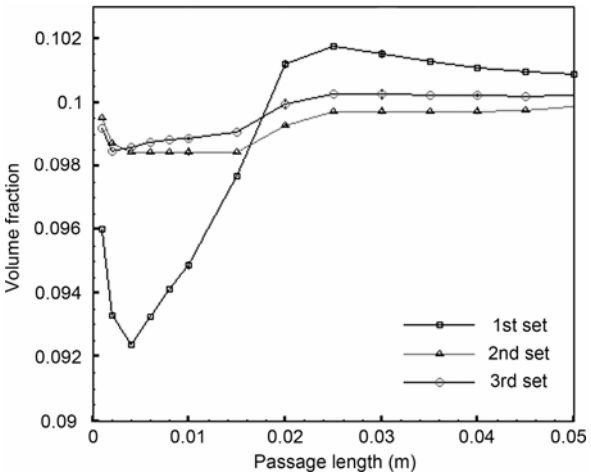

Figure 13 Particle volume fraction distribution in different locations.

ablating velocity on passage walls) mainly influences the general removal rate, while influence on ablating location mostly comes from variation of granular pressure.

According to eq. (15), product of granular pressure and particle velocity is in proportion to ablating rate. Because Preston coefficient is an experimentally determined constant, this R/K_p can be considered as a measurement of ablating rate. Record $\boldsymbol{Q}=1/K_p$ as a characteristic value to deduce a dimensionless ablating rate $\boldsymbol{R}^+$, stated as

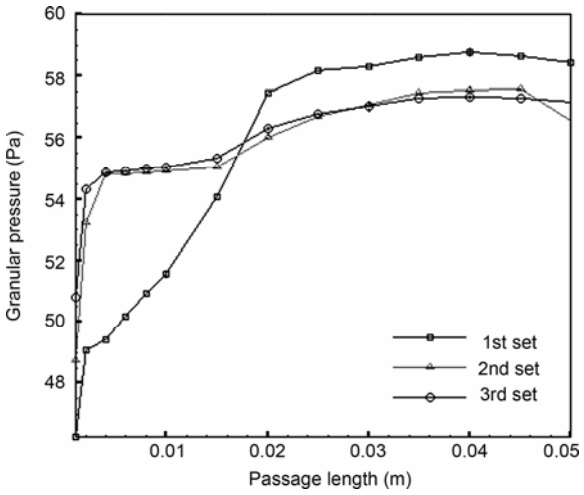

Figure 14 Granular pressure distribution in different locations.

$$\boldsymbol{R}^+ = \boldsymbol{V} \cdot \boldsymbol{P}. \tag{18}$$

Based on the theory mentioned above, it can be known that with n sampling points along the passage, ablating rate samples under m samples of velocities can be collected in a matrix (obviously, here in this simulation m is 10 and n is 15), stated as

$$\begin{aligned}\boldsymbol{R}^+_{m\times n} &= \boldsymbol{V} \cdot \boldsymbol{P} \\ &= \begin{bmatrix} v_1 \\ v_2 \\ \vdots \\ v_m \end{bmatrix} \cdot \begin{bmatrix} p_1 & p_2 & \cdots & p_n \end{bmatrix} \\ &= \begin{bmatrix} r^+_{11} & r^+_{12} & \cdots & r^+_{1n} \\ r^+_{21} & r^+_{22} & \cdots & r^+_{2n} \\ \vdots & \vdots & \ddots & \vdots \\ r^+_{m1} & r^+_{m2} & \cdots & r^+_{mn} \end{bmatrix}. \end{aligned} \tag{19}$$

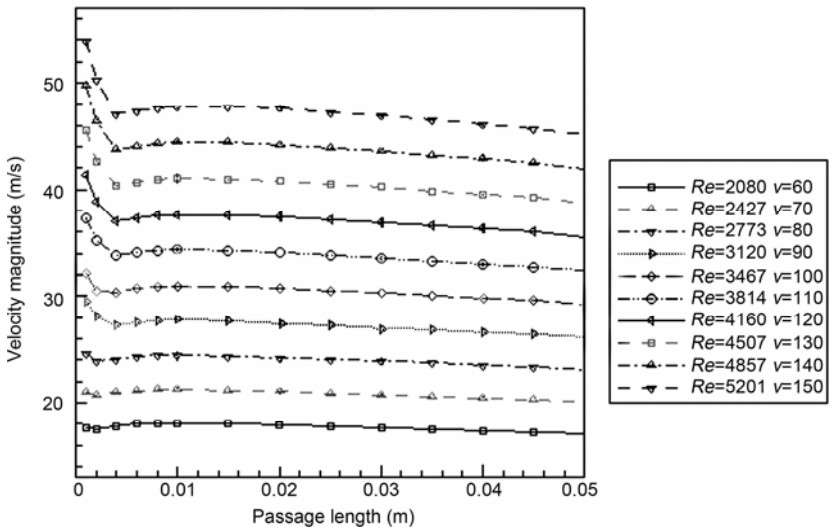

Figure 15 Velocity distribution under different Reynolds numbers.

Figure 16 states dimensionless ablating rate distribution under different Reynolds numbers. As a mensuration of machining results, this $\boldsymbol{R}^{+}$ helps in analysis and indications in flow field environment characters, setting of initial parameters, and geometry structure of passage and restrained module. It can be seen from the figure that under dual action of both granular pressure and particle velocity, characteristics of ablating rate distribution under different Reynolds numbers are:

(1) Ablating degree of particles accords with an "increase-and-decrease" pattern. It means that under only one flow rate, ablating situation along the passage can never be equal. Normalization here may help analyze and predict machining results, and give a suggestion on velocity chosen in machining process. While to get better machining results, control of flow rate is unavoidable.

(2) Ablating rate curve turns out to have these following characteristics: ablating rate generally tends to grow along the passage; with this tendency, its peak region translates towards the after part of passage, and the range of peak region of ablating rate extends. From the above it can be deduced that, different Reynolds numbers primarily have controls on different ablating regions. Therefore, given ablating rate sample matrix $\boldsymbol{R}$, by changing abrasive flow rate and corresponding working time, object of equilibrium machining in the whole passage can be realized.

Elements in ablating rate sample matrix $\boldsymbol{R}$ can be determined after a test for measurement Q.

For ablating process, use matrix $\boldsymbol{t}=\begin{bmatrix} t_1 & t_2 & \cdots & t_m \end{bmatrix}$ to represent machining time, where t_j stands for time taken when working with abrasive flow under an inlet velocity of j.

Final machining quantities composes a column matrix $\boldsymbol{w}$ with n elements, and all the elements are equal to final ablating quantity W, as

$$\boldsymbol{w}=\boldsymbol{t}\cdot\boldsymbol{R}=\begin{bmatrix} W & W & \cdots & W \end{bmatrix}^{\mathrm{T}}. \tag{20}$$

Thus, given only final ablating quantity W in the machining, it is practicable to deduce machining time matrix $\boldsymbol{t}$, and then corresponding machining procedure should be:

$$\boldsymbol{t}=\boldsymbol{w}\cdot\boldsymbol{R}^{-1}. \tag{21}$$

The more velocities and sample points chosen, the more elements deduced in that time control matrix, and the better the final machining quality it will gain. Meanwhile, this method allows to quantify trade-offs between machining efficiency and quality, and thus can meet different requirements in the processing.

3.3 Simulation of near-wall particle trajectories

Since interval distance between machining surface and restrained module is quite short (0.8 mm), formation of wall turbulence is restricted. The abrasive particles in working are mainly located in laminar sublayer in turbulence coherent structure. y^{+} contour with a Reynolds number of 4507 is shown in Figure 17. It can be seen from the figure that near-wall y^{+} equals approx 1. According to the findings of turbulence boundary layer coherent structure by Blackwelder, low-speed stripes are actually traces of stream-wise vortex [23, 24]. Stream-wise vortex plays a crucially importance part in generation and transport of turbulence energy, as well as in turbulence development [25]. For this reason, an injection of abrasive particles is set at inlet surface for the simulation of their trajectories along the passage. Projection of one near-wall trajectory ($y^{+}\approx1$) on YZ plane is shown in Figure 16.

Figure 18 proves that near-wall particle track follows the path of a stream-wise vortex. And its longitudinal velocity is reduced due to friction as particle approaching the wall. It

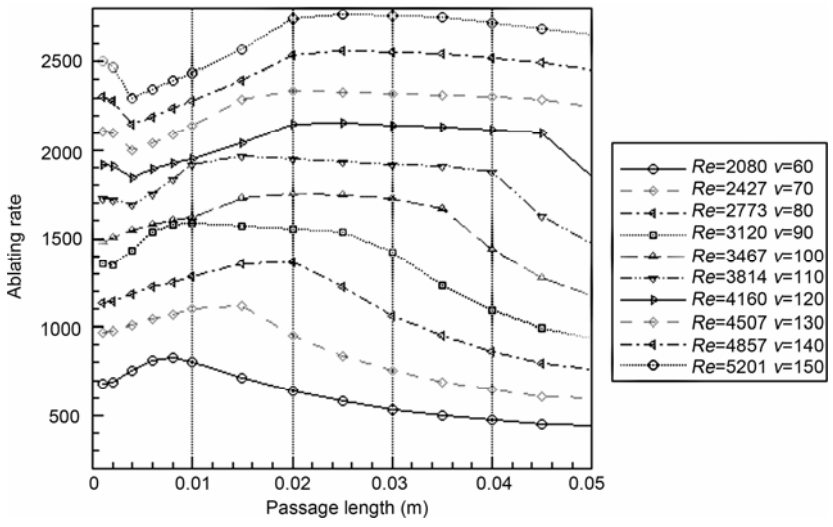

Figure 16 Dimensionless ablating rate distribution under different Reynolds numbers.

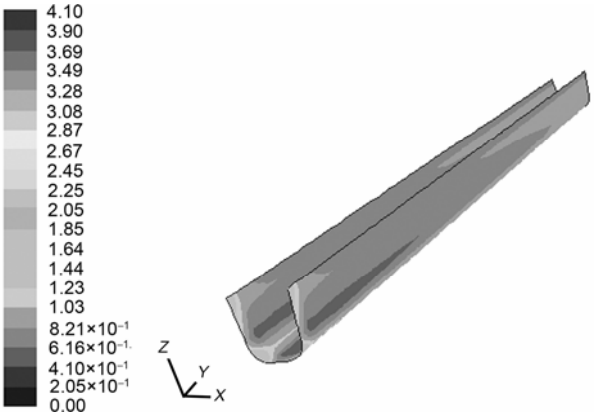

Figure 17 y^+ contour with *Re*=4507.

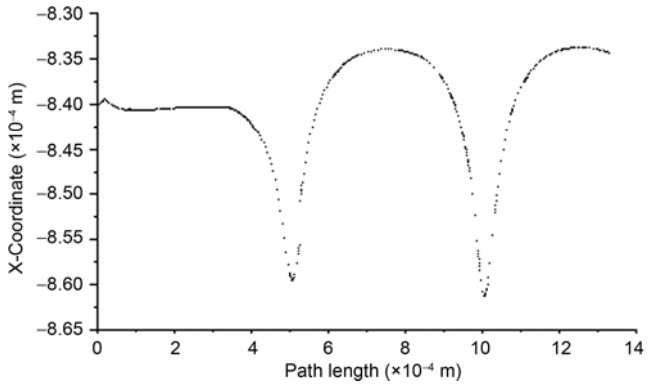

Figure 18 Projection of one near-wall trajectory on *YZ* plane.

can be concluded that the particle following a stream-wise vortex will leave marks angled with longitudinal direction on the wall. Multifarious directions of marks guarantee randomness of abrasion, which meets the machining requirements mentioned before.

In addition, Reynolds stress is primary generated by sweep down flow given the condition $y^+<5$. Particles in these areas are much more likely to generate flows towards the wall. This property is evidently a significant factor in development of machining efficiency and quality.

4 Conclusion

This paper presented a DPM for particle motions in a SAFM passage. With this model, particle volume fraction, turbulence fluctuating kinetic energy and granular pressure exerted on different near-wall areas in the passage are examined and analyzed. Based on the results, conclusions are drawn below.

(1) After particles enter the passage, along with turbulence development and particle deposition, particle phase will tend to be well-distributed after a period of time. However, increase of Reynolds number, namely increase of inlet velocity, can cause difficulties in this procedure.

(2) Granular pressure is principally affected by volume fraction of particle phase, with a variation tendency similar to the latter. Furthermore, flows with higher Reynolds number tend to have larger granular pressure due to their advantages in turbulence kinetic energy. But meanwhile, affected by dynamic pressure of particle phase, granular conductivity will be weakened and ultimately leads to a fall-back of granular pressure. Yet velocity of near-wall particles is not affected much, only in the change of general value. Abrasive flow machining process mainly appears as translation of ablating location with influence by granular pressure, and as variation of machining efficiency with influence by near-wall particle velocity. Via control of inlet velocity (or Reynolds number instead) and its corresponding machining time, it is supposed to work out machining process according to machining requirements.

(3) In different tangential locations, the trend of granular pressure distribution curve is generally the same. Since on sidewalls particle distribution and turbulence generation are more likely to reach a stable phase, and its granular pressure will distribute better, the machining results will be better. Therefore efficiency on bottom walls should be considered first in this research.

(4) Since during abrasion procedure abrasive particles are mostly located in laminar sublayer of turbulence boundary layer, trajectories of near-wall particles are tracked during the simulation. Results prove that near-wall abrasive particles follow the track of a stream-wise vortex, which provides a strong evidence for randomness of cutting direction. In addition, particle motion in this area is primarily influenced by sweep-down flow. This phenomenon benefits a lot to impact of particles against the wall. These conclusions reaffirm the feasibility of the SAFM method.

This work was supported by the National Natural Science Foundation of China (Grant Nos. 50875242, 50905163) and Key Project of Natural Science Foundation of Zhejiang Province (Grant Nos. Z107517, Y1090836).

1 Chen Y S, Shan X W, Chen H D. New direction of computational fluid dynamics and its applications in industry. Sci China Ser E-Tech Sci, 2007, 50(5): 521–533
2 Jin J, Liu P Q, Lin G P. Numerical simulation of heat transfer of latent functionally thermal fluid in tubes with coaxially inserted cylindrical bars in laminar. Sci China Ser E-Tech Sci, 2008, 51(8): 1232–1240
3 Jain V K, Adsul S G. Experimental investigations into abrasive flow machining (AFM). Int J Mach Tool Manu, 2000, 40(7): 1003–1021
4 Guo Y Z. Application of abrasive flow machining in manufacture of aeroengine (in Chinese). Aeronaut Manu Tech, 1993. 5: 28–32
5 Rhoades L J. Abrasive flow machining: a case study. J Mater Process Tech, 1991, 28(2): 107–116
6 Madadnia J, Reizes J A. Feasibility study of using cavitation to increase erosion in particulate-laden water jet cutting devices. Int Conf Abrasive Tech. W Sci P Co Pte Ltd, 1999
7 Jones A R, Hull J B. Ultrasonic flow polishing. Ultrasonics, 1998, 36: 97–101
8 Wang C. Study and comparison of vibrative polishing (in Chinese). OR Tran, 1996, 5(2): 5–9

9 Jha S, Jain V K. Design and development of the magnetorheological abrasive flow finishing (MRAFF) process. Int J Mach Manu, 2008, 48: 415–426
10 Shirolkar J S, Coimbra C F M. Fundamental aspects of modeling turbulent particle dispersion in dilute flows. Prog Energy Combust Sci, 1996, 22: 363–399
11 Kallio G A, Stock D E. In Gas–Solid Flows. ASME FED, 1986, 35: 23
12 Mostafa A A. On the interaction of particles and turbulent fluid flow. Int J Heat Mass Tran, 1987, 30 (12): 2063–2075
13 Crowe C T. Review: Numerical models for dilute gas-particle flows. Trans ASME I: J Fluid Eng, 1982, 104: 297–303
14 Booij S M, van Brug H, Braat J J M. Nanometer deep shaping with fluid jet polishing. Opt Eng, 2002, 4(8): 1926–1931
15 Fang H, Guo P J, Yu J D. Optimization of the material removal in fluid jet polishing (in Chinese). Opt Tech, 2004, 30(2): 248–250
16 Toshio T, Paul D F. Micromechanics of diamond composite tools during grinding of glass. Mater Sci Eng, 2000, A285: 69–79
17 Burry D, Bergeles G. Dispersion of particles in anisotropic turbulent flows. Int J Multiphase Flow, 1993, 19: 651–664
18 Kader B. Temperature and concentration profiles in fully turbulent boundary layers. Int J Heat Mass Tran, 1981, 24(9): 1541–1544
19 Gatzen H H, Wu K H, Cvetkovic S. Modeling CMP – Investigation of the mechanical removal mechanism, Proc. ASPE 20th Ann Meet, Norfolk, Virginia, USA, 2005, 500–503
20 Kumar S, Hart D. Granular pressure measurement in fluidized beds. ASME Cavitation and Multiphase Flow Forum, 1990, FED–98: 1–6
21 Nikuradse J. Laws for Flows in Rough Pipes. Technical Report, NACA Technical Memorandum 1292. National Advisory Commission for Aeronautics, Washingyon DC, 1950
22 Gevrin F, Masbemat O. Granular pressure and particle velocity fluctuation predictions in liquid–solid fluidized beds. Chem Eng Sci, 2008, 63 (9): 2450–2464
23 Blackwelder R F, Kaplan R E. Streamwise vortices associated with the bursting phenomenon. J Fluid Mech J Fluid Mech Digit Arch, 1976, 94: 577–594
24 Zhou M D, Liu D P, Blackwalder P F. An experimental study of receptivity of acoustic waves in laminar boundary layers. Exp Fluids, 1994, 17: 1–9
25 Kai L, Zhang N, Lu L P. Production of streamwise vortexes in a turbulent boundary layer (in Chinese). J Beijing Univ Aeronaut Astronaut, 2005, 31(110): 1800–1803